



Synthesis and characterization of low-cost carbon nanotubes by chemical vapor deposition for aluminum removal from aqueous solution

Alfarooq O. Basheer^{a,*}, Marlia M. Hanafiah^{a,b}, Mohammed Abdulhakim Alsaadi^{d,e},
Wan Zuhairi Wan Yaacob^c, Y. Al-Douri^{d,f}, A. Bouhemadou^g

^aDepartment for Earth Sciences and Environment, Faculty of Science and Technology, Universiti Kebangsaan Malaysia, 43600 Bangi, Selangor, Malaysia, emails: farooqaltalib@gmail.com (A.O. Basheer), mhmarlia@ukm.edu.my (M.M. Hanafiah)

^bCentre for Tropical Climate Change System, Institute of Climate Change, Universiti Kebangsaan Malaysia, Bangi 43600, Selangor, Malaysia

^cGeology Programme, School of Environmental and Natural Resource Sciences, Faculty of Science and Technology, Universiti Kebangsaan Malaysia, 43600 Bangi, Selangor, Malaysia, email: drwzwy@gmail.com

^dNanotechnology and Catalysis Research Center (NANOCAT), University of Malaya, 50603 Kuala Lumpur, Malaysia, emails: mdsd68j@gmail.com (M.A. Alsaadi), yaldouri@yahoo.com (Y. Al-Douri)

^eNational Chair of Materials Science and Metallurgy, University of Nizwa, 611 Nizawa, Oman

^fDepartment of Mechatronics Engineering, Faculty of Engineering and Natural Sciences, Bahcesehir University, 4349 Besiktas, Istanbul, Turkey

^gLaboratory for Developing New Materials and their Characterizations, Department of Physics, Faculty of Science, University Ferhat Abbas Setif 1, Setif 19000, Algeria

Received 23 November 2019; Accepted 1 November 2020

ABSTRACT

This study investigates novel multi-walled carbon nanotubes (MWCNTs) grown on agricultural waste, using loaded iron nanoparticles as catalyst templates and acetylene as carbon source through chemical vapor deposition under specific conditions, to wit: 550°C reaction temperature, 47 min reaction time, and 1 gas ratio. The specifications of MWCNTs are analyzed and characterized with the use of field-emission scanning electron microscopy, energy-dispersive X-ray spectroscopy, transmission electron microscopy, Fourier-transform infrared spectroscopy, X-ray diffraction, thermogravimetric analysis, Brunauer–Emmett–Teller surface area analysis, and zeta potential analysis. The results reveal that MWCNTs have high quality and unique morphologies. The removal and capacity of Al³⁺ are optimized through response surface methodology, whilst the adsorption kinetics results are well ascribed to the pseudo-second-order model, the isotherm data are effectively fitted using a Langmuir model. The maximum adsorption capacity is 393.52 mg/g. The results demonstrate that MWCNTs can be regarded as a new low-cost adsorbent in wastewater treatment for the removal of Al³⁺.

Keyword: Carbon nanotubes; Chemical vapor deposition; Response surface methodology; Adsorption

1. Introduction

Relentless industrialization and infrastructure development have led to progressive environmental degeneration. Pollutants, including industrial waste, agricultural

run-off and wastewater discharge, sewage, are primary contributors to environmental contamination and contain deadly substances, such as metallurgical toxins, and other organic and inorganic poisons. Specifically, metal-based pollution is generated as a consequence of industrial effluence being released into the environment via water sources.

* Corresponding author.

The resultant damage threatens not merely human welfare and existence, but all life on Earth. Aluminum is particularly reactive to both oxygen and carbon. Moreover, it has the potential to cause significant damage to human health and has been implicated in the development of autistic spectrum disorders, Alzheimer's disease, and neurotoxicity of the central nervous system [1].

According to the Environmental Protection Agency, the concentration of aluminum in potable water must not be permitted to pass 0.05–0.20 mg/L [2]. This suggests that it is necessary to eliminate aluminum from waste prior to any discharge which might reach natural water sources.

There are multiple techniques which are currently utilized for the removal of metals from wastewater, including chemical precipitation with hydroxides, chelating precipitation with sulfides, ion exchange, bioadsorbents, adsorption using porous carbon materials, electrodialysis, coagulation and flocculation, membrane filtration, flotation, and electrochemical treatment [3–7].

The technique of choice is currently deemed to be adsorption using porous carbon materials due to its relative inexpensiveness, its applicability for large-scale use, the ease with which it can be employed, and its inherent adaptability. Typically, adsorbents use comprised of elements such as sawdust [8], rice husks [9], maize cobs [10], granulated blast furnace slag [11], kaolinitic and Giru clays [12], aquatic plants [13], powdered activated carbon (PAC) [14], and nanomaterials [15].

The use of nanomaterials has been widely investigated due to the excellent mechanical performance of these materials. Carbon nanotubes (CNTs) have been widely used and evaluated in water treatment as a consequence of their unique structure, small size, catalytic potential, high reactivity, easy separation, and large surface area, all of which render them an effective adsorbent for many metals. CNTs have been developed using several methods, including chemical vapor deposition (CVD), laser ablation, and arc discharge. CVD is superior thanks to its cost-effectiveness and ability to produce high-purity materials under controlled growth conditions.

PAC is considered the ideal substrate for CVD because of its wide precursor accessibility, low-cost, and chemical alteration potentials. Selective growth is comparatively easy to achieve through synthesis using pre-patterned catalyst nanoparticles, such as iron, nickel, molybdenum, aluminum, cobalt, and zirconium. Research by Xiang et al. [16] and Aljumaily et al. [17] resulted in the successful synthesis of CNTs on PAC via CVD through the use of acetylene as a carbon source with several catalysts produced from iron, cobalt, aluminum, and nickel. Moreover, Alayan et al. [18] synthesized carbon nanomaterials (CNMs) on commercial PAC loaded with nickel nanoparticles by using methane as a carbon source and Yahyazadeh and Khoshandam synthesized CNTs via CVD on silicon sheets loaded with iron by utilizing methane as a carbon source. Research by Zhao et al. [20] has demonstrated that high yields of CNTs can be synthesized in water through CVD by using iron and molybdenum catalysts supported on a magnesium oxide substrate. An inverse correlation between catalyst lifetime and CNT growth rate was observed by Chen et al. [21]. Furthermore, Mamun et al. [22] have reported that PAC can

function as a useful precursor for CNT growth. Interestingly, when compared to other substrates, PAC does not need to be chemically or physically removed from the functional bulk material. Catalyst iron nanoparticles with acetylene as a carbon source can provide CNTs with high quality, increased density, and enhanced purity. Having reviewed the relevant literature in this field, the researcher intends that the current study will offer insights into the growth of unique multi-walled carbon nanotubes (MWCNTs).

This research investigates the use of synthesized MWCNTs on PAC as an agrarian effluence precursor when loaded with iron nanoparticles using CVD. Several techniques are adopted in order to identify and evaluate the structural and morphological properties of MWCNTs, to wit: energy-dispersive X-ray spectroscopy (EDX), field-emission scanning electron microscopy (FESEM), transmission electron microscopy (TEM), X-ray diffraction (XRD), Fourier-transform infrared spectroscopy (FTIR), thermogravimetric analysis (TGA), Brunauer–Emmett–Teller (BET) analysis, and zeta potential analysis. The results indicate that it is possible to divorce MWCNTs from the water with comparative ease due to their hydrophobicity. This suggests that this procedure might comprise a scalable process with applicability to industrial waste management, both due to its ease of operation and its superior removal performance. Moreover, MWCNTs are also a relatively inexpensive adsorbent. Response surface methodology (RSM), with central composite design (CCD), is adopted to optimize Al^{3+} removal. Adsorption kinetics and isotherm models are extensively evaluated and discussed.

2. Experimental

2.1. Materials and reagents

Iron(III) nitrate nonahydrate $Fe(NO_3)_3 \cdot 9H_2O$ and acetone are purchased from Friendemann Schemicit, Malaysia. Aluminum standard solution $Al(NO_3)_3 \cdot 9H_2O$, hydrochloric acid (HCl), sodium hydroxide (NaOH) are obtained from Merck (Malaysia). C_2H_2 , H_2 and N_2 are used for MWCNTs growth are purchased from Alpha Gas Solution (AGS), Malaysia. The agricultural wastes PAC which have been fabricated by our group is utilized to synthesis MWCNTs [23].

2.2. Synthesis MWCNTs

2.2.1. Catalyst impregnation

Fe was utilized as a catalyst and added in 5 mL acetone, then mixed with (2 g) PAC. However, the mixture is sonicated at 60°C for 99 min till acetone evaporated. Subsequently, sample bio-PAC/Fe is dried at 105°C for 24 h. Calcinated PAC/Fe at 400°C at 2 h under inert gas (purified N_2 , 200 mL/min) [24].

2.2.2. CVD growth

CNTs growth is carried out by placing (300 mg) PAC/Fe in a ceramic boat with in CVD reaction tube. Typical growth is accomplished by reduction under H_2 at 550°C with the flow (160 mL/min). Thereafter, C_2H_2 is used as a carbon source and mixed with H_2 at a 1:4 ratio. The reaction

is passed through a heated reactor at 47 min. After the MWCNTs growth sample is slowly cooling under purified N_2 flow rate (200 mL/min) to room temperature, the MWCNTs sample is collected after the completion of the reaction.

2.3. Characterizations

Surface morphology for MWCNTs is characterized by FESEM with EDX, model ZEISS (Merlin, UK), and TEM, (Hitachi-HT7700, Japan). FTIR is utilized in order to analyze both surface functional groups and chemical bonds (Perkin Elmer, USA). The structural phase is analyzed relying on the powder XRD by a Burker AXS D8 advance (Germany). Whereas the determination of thermal oxidation is obtained from the TGA using STA-6000 thermal analyzer (Perkin Elmer, USA). Moreover, the pore size and surface area are calculated by the BET method (TriStar II 3020, USA). Lastly, Zeta potential is utilized for surface charge measurement (Zetasizer, UK).

2.4. Adsorption study

2.4.1. Kinetic and isotherm adsorption

The kinetic study specifies the crucial features of the ions transfer rate, from the solution to the surface of adsorbents, and its associated aspects. For the sake of determining the potential adsorbent application, the kinetic adsorption process is relied on to specify the adsorbent competence [25]. The setting of the adsorbent dosage and the pH parameters attains the kinetic study. Meanwhile, the Al^{3+} ion concentrations varied in their values (3 and 5 mg/L) when the kinetic behavior is being studied and they are managed at various contact times pending on the equilibrium state that is reached at 92 min. Three known kinetic models are adapted in the present research namely, the pseudo-first-order, pseudo-second-order and the intraparticle diffusion model. The optimum condition of pH, amount of MWCNTs dosage and contact time are obtained into consideration when conducting the isotherm study along with the optimization study. Freundlich and Langmuir's models are the most known in the isotherm study [26]. Both models tend to depict the Al^{3+} adsorption processes on MWCNTs surface where the primary concentration of Al^{3+} is varied from 3 to 40 mg/L.

3. Results and discussion

3.1. Characterization of MWCNTs

The morphologies and structures of synthesized MWCNTs are determined through FESEM prior to and after fabrication. Figs. 1a and b demonstrate that FESEM images with different magnifications can be observed before growth activated carbon (AC/Fe). The substrate surface is rough, and the catalyst is dispersed. Figs. 1c and d reveal that there is a carpet-like deposit containing highly dense MWCNT arrays without evident catalyst impurities following growth. The diameter of the nanotubes ranged from 34.18 nm to 37.45 nm. TEM images confirmed that MWCNTs possess successful structure formation and high quality.

EDX analysis determined the substrate elements prior to and following growth. Fig. 2a shows that the EDX spectra have indicated that the catalyst is successfully embedded on the AC/Fe surface. The surface of MWCNTs contained 97.8% carbon after growth with other impurities either decreasing or disappearing, as illustrated in Fig. 2b.

Fig. 3a illustrates the fundamental traits of the functional groups, in addition to the surface chemistry, all of which were revealed through the application of FTIR. The weak peaks at 3,747 and 3,593 cm^{-1} can be attributed to either the O–H stretching vibration of the hydroxyl group or to the adsorption of some atmospheric water during FTIR measurements on the surface of MWCNTs [27]. At 3,022 and 2,819 cm^{-1} , the two broad peaks can be assigned to the C–H stretching vibration, with the sharp peak of 2,072 cm^{-1} indicating the $C\equiv C$ stretching vibrations [28]. The sharp peak of 1,685 cm^{-1} may be attributed to C=C with C=O conjugation or the interaction of the skeletal MWCNTs and carboxyl or even ketone groups [29]. A strong and sharp peak located at 1,552 cm^{-1} is attributed to the C=O conjugation resulting from the stretching mode of the functional groups on the surface of MWCNTs that originated from the hybridized carbon [30]. The peaks of 1,365 and 1,238 cm^{-1} can be assigned to the N–N and CH–CH₃ bonds caused by the intercalated N atoms between the graphite layers of the nanotube walls. The band at 1,127 cm^{-1} indicated the C–O stretching vibrations in alcohols, phenols, and ether or ester groups [31,32]. A sharp peak at 867 cm^{-1} is assigned to the CH₃ group vibration. Fig. 3b shows the XRD patterns of MWCNTs. XRD is an accelerated analytical method mainly utilized to identify crystalline and molecular structural materials, which can provide information on unit cell dimensions. The strongest diffraction peak, at $2\theta = 25.7^\circ$, corresponds to the (002) reflection associated with the crystalline and cylinder structures [33]. The peaks of $2\theta = 33.37^\circ$ and 43.47° correspond to the (100) and (101) orientations, respectively. All peaks were well matched with the hexagonal graphite structure.

TGA is employed to gauge thermal stability in the MWCNTs, as indicated in Fig. 3c. Moreover, there is a small weight loss arising from the elimination of water at around 200°C, as revealed in the TGA curve. The existing weight loss is a consequence of the loss of carbon and the oxidation of the nanotubes at 650°C–750°C. Decomposition of the formed carbonaceous material is signified by the weight reduction, which commences at 650°C. As noted in Fig. 4, these findings have been verified via the FTIR spectra. There are multiple factors that determine the activation energy of MWCNT oxidation. These include the quantity of walls, the defects, and the existence of impurities. According to Misra et al., it is possible to observe comparable findings in the TGA profiles [35]. The fact that no composition was recorded when the temperature passed 1,000°C indicates that the MWCNTs can be regarded as possessing thermally stability.

It is essential that an evaluation of the surface temperature is performed. Specifically, the BET surface area appraisal can be employed to enhance understanding of the surface structure of the synthesized MWCNTs. As indicated in Fig. 3d, nitrogen adsorption/desorption of MWCNTs exhibits typical IV-type curves with

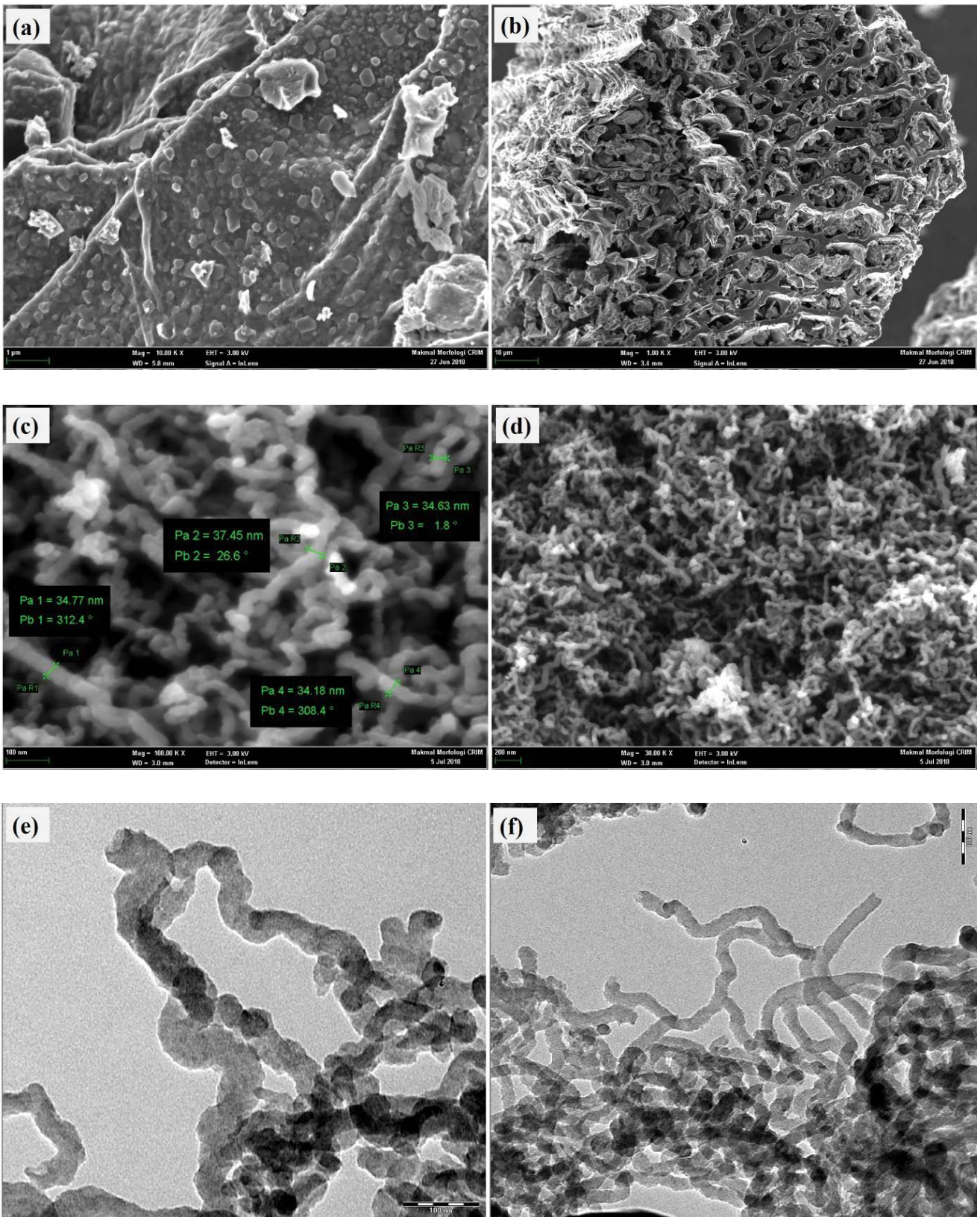


Fig. 1. Field-emission scanning electron microscopy images (a and b) before growth, (c and d) MWCNTs and transmission electron microscopy images (e and f) of MWCNTs.

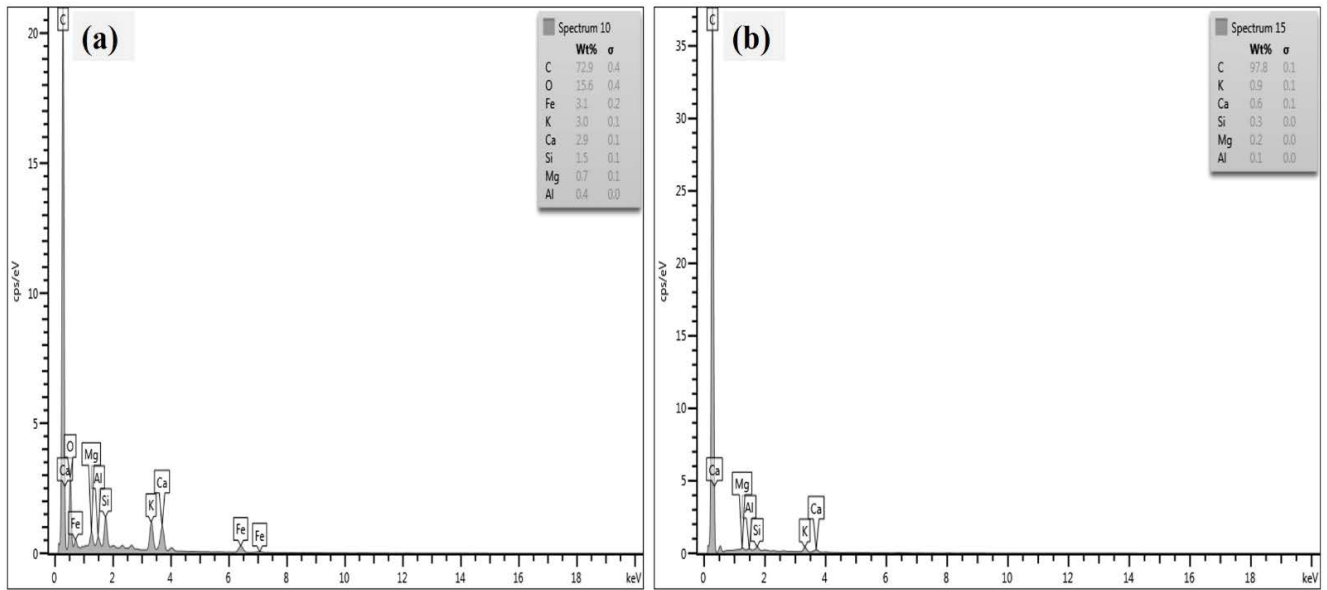


Fig. 2. Energy-dispersive X-ray spectra (a) AC/Fe before growth and (b) after growth.

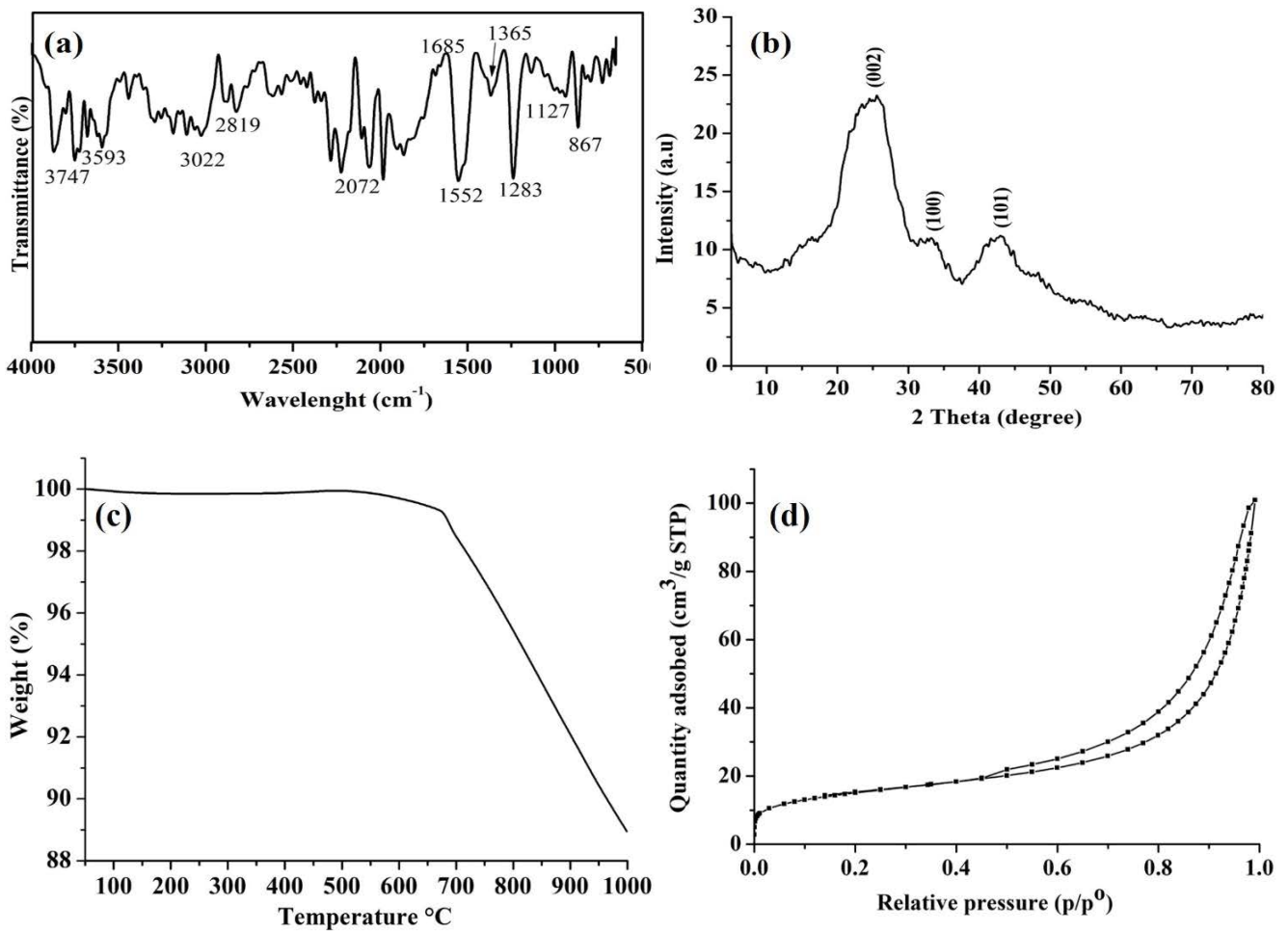


Fig. 3. Plots of MWCNTs (a) Fourier-transform infrared spectroscopy spectra, (b) X-ray diffraction analysis, (c) thermogravimetric analysis curve and (d) N₂ adsorption-desorption isotherms.

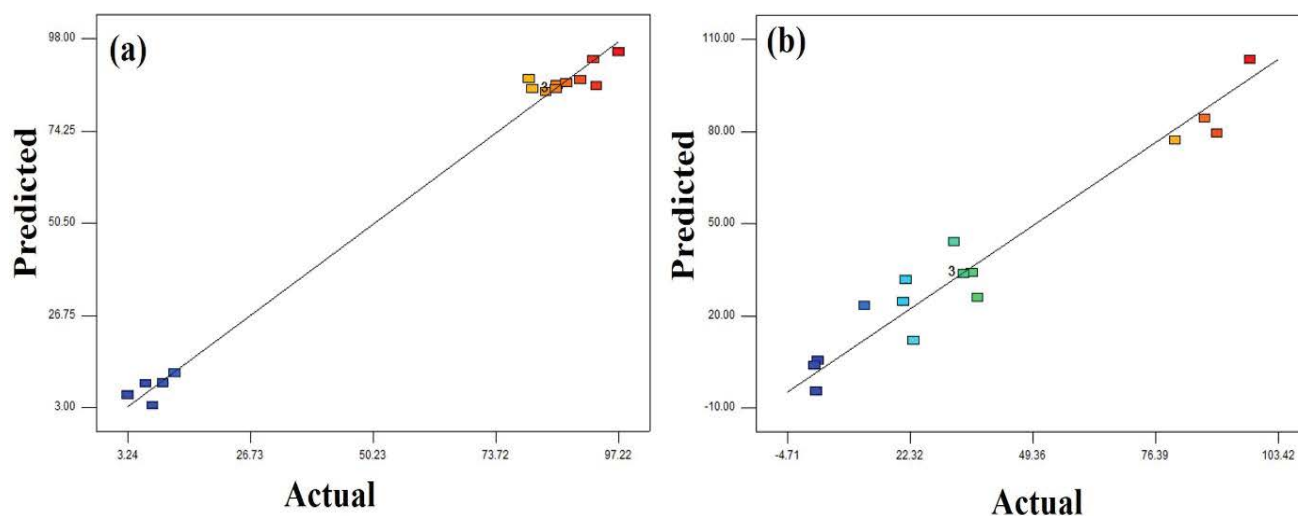


Fig. 4. Predicated vs. experimental data for Al^{3+} (a) removal (%) and (b) capacity (mg/g) on MWCNTs adsorbent.

hysteresis loops for the relative pressure (P/P^0) range of 0.5–1.0. In accordance with the BET surface area, the results show that the total surface area is $54.26 \text{ m}^2/\text{g}$, the pore volume is $0.156 \text{ m}^3/\text{g}$, and the pore size is 11.5 nm . Further, this was in keeping with the results of the morphological analyses [34].

Zeta potential is crucial both to the classification of surface behavioral features in the provided aqueous solutions and to the assessment of suspension stability. Consequently, zeta potential analysis is conducted in order to gauge the electrical potential on the surface of the MWCNTs. The zeta potential of various samples, and the differences between them, are determined under numerous pH levels. When MWCNTs (10 mg) were spread in 20 mL in a pH range of 3–11, zeta potential values between 0.440 mV to and 0.0712 mV were recorded. The surface charge of MWCNTs is positive in an acidic medium ($\text{pH} < \text{pHpzc}$). Although the surface charge was negatively reduced when $\text{pH} > \text{pHpzc}$, resulting in the easy interaction of positive ions and the surface of MWCNTs, thereby influencing the high adsorption as a result of electrostatic interaction.

3.2. Optimization

3.2.1. Experimental design for optimization of Al^{3+} adsorption

RSM is utilized to optimize the removal of Al^{3+} . The current study has thoroughly investigated the impact of interaction amongst independent factors on the adsorption of MWCNTs under 5–20 mg adsorbent dosage, pH 3–11, and with a 10–120 min contact time. Table 1 presents the actual parameters of each run using the Design-Expert software. In this optimization, the initial concentration was reduced to 5 mg/L and the flasks were agitated in a shaker at 180 rpm [35].

Seventeen experimental runs are conducted to examine the optimal adsorption factors using RSM. The CCD technique has been utilized to conduct experiments in the current study, a technique which is widely employed to predict more accurate values in relation to the actual responses. Nonetheless, CCD are very efficient, providing

much information on experiment variable effects and overall experimental error in a minimum number of required runs. [36]. The removal and capacity of responses are taken into consideration in the design, as per Table 1. The highest removal and capacity are 97% and 90.6 mg/g under a 5 mg/g adsorbent dosage, pH 10, and with a 120 min contact time. The experimental and predicted values are close to the correlation (R^2) of the Al^{3+} removal (%) and capacity (mg/g), which are found to be 0.97% and 0.9453 mg/g, respectively.

The analysis of variance results for the responses are indicated in Tables 2 and 3. The F -values of the two models are 95.76 and 13.44 in respect of removal and capacity. This result suggests that the two models are significant. In addition, $p < 0.0500$ confirms that the two models are highly significant. Data analysis provides the expressions for the responses using the following equations:

$$\text{Removal} = +84.95 - 1.17A + 40.55B + 0.97C + 0.94AB - 0.74AC + 3.06BC + 0.51A^2 - 38.19B^2 + 1.75C^2 \quad (1)$$

$$\text{Capacity} = +33.65 - 29.83A + 15.13B + 9.11C - 4.38AB - 11.51AC - 7.46BC + 20.70A^2 - 14.69B^2 + 1.28C^2 \quad (2)$$

where A is MWCNTs dosage, B is pH, and C is contact time

Figs. 4a and b present the theoretical and the experimental lab values for the removal (%) and capacity (mg/g), respectively. The optimum predicted conditions values are comparable to the lab experimental values.

Fig. 5a illustrates the 3D surface plot interaction effects of MWCNTs dosage and pH on adsorption processes in terms of removal (%) and capacity (mg/g). The impact of adsorbent dosage and pH on adsorption are also significant. There is a correlation between the degree to which the adsorbent increases and the concentration of the dynamic sites. Thus, the electrostatic charge of the adsorbed solution is regulated in accordance with the desired adsorption level through the elimination of the competitive H^+ cations. Adsorbent dosage increases in direct accordance

Table 1
List of design of experiments runs and the actual values obtained from each response

Run	Factors			Responses	
	Dosage (mg/g)	pH	Time (min)	Removal (%)	Capacity (mg/g)
1	5.00	11.00	10.00	80.72	80.72
2	20.00	3.00	120.00	7.96	1.99
3	12.50	7.00	65.00	85.22	34.088
4	12.50	7.00	65.00	85.22	34.088
5	12.50	7.00	10.00	92.96	37.184
6	5.00	7.00	65.00	87.2	87.2
7	20.00	11.00	120.00	92.4	23.1
8	12.50	7.00	120.00	80.04	32.016
9	12.50	3.00	65.00	3.24	1.296
10	20.00	3.00	10.00	6.64	1.66
11	12.50	7.00	65.00	85.22	34.088
12	20.00	7.00	65.00	83.32	20.83
13	12.50	11.00	65.00	89.88	35.952
14	5.00	3.00	10.00	12.24	12.24
15	5.00	3.00	120.00	10.02	89.88
16	20.00	11.00	10.00	85.36	21.34
17	5.00	11.00	120.00	97.22	97.22

Table 2
Analysis of variance for Al³⁺ removal on multi-walled carbon nanotubes

Source	Sum of squares	Degree of freedom	Mean square	F-value	P-value Prob. > F
Model	22,208.45	9	2,467.61	95.76	<0.0001
A-dose	13.74	1	13.74	0.53	0.4890
B-pH	16,441.40	1	16,441.40	638.06	<0.0001
C-contact time	9.45	1	9.45	0.37	0.5639
AB	6.99	1	6.99	0.27	0.6185
AC	4.38	1	4.38	0.17	0.6924
BC	74.66	1	74.66	2.90	0.1325
A ²	0.69	1	0.69	0.027	0.8742
B ²	3,907.76	1	3,907.76	151.65	<0.0001
C ²	8.20	1	8.20	0.32	0.5903

Table 3
Analysis of variance for Al³⁺ capacity of multi-walled carbon nanotubes

Source	Sum of squares	Degree of freedom	Mean square	F-value	P-value Prob. > F
Model	15,080.63	9	1,675.63	13.44	0.0012
A-dose	8,900.68	1	8,900.68	71.41	<0.0001
B-pH	2,288.14	1	2,288.14	18.36	0.0036
C-contact time	829.23	1	829.23	6.65	0.0365
AB	153.39	1	153.39	1.23	0.3039
AC	1,059.15	1	1,059.15	8.50	0.0225
BC	445.66	1	445.66	3.58	0.1005
A ²	1,147.84	1	1,147.84	9.21	0.0190
B ²	578.38	1	578.38	4.64	0.0482
C ²	4.41	1	4.41	0.035	0.8561

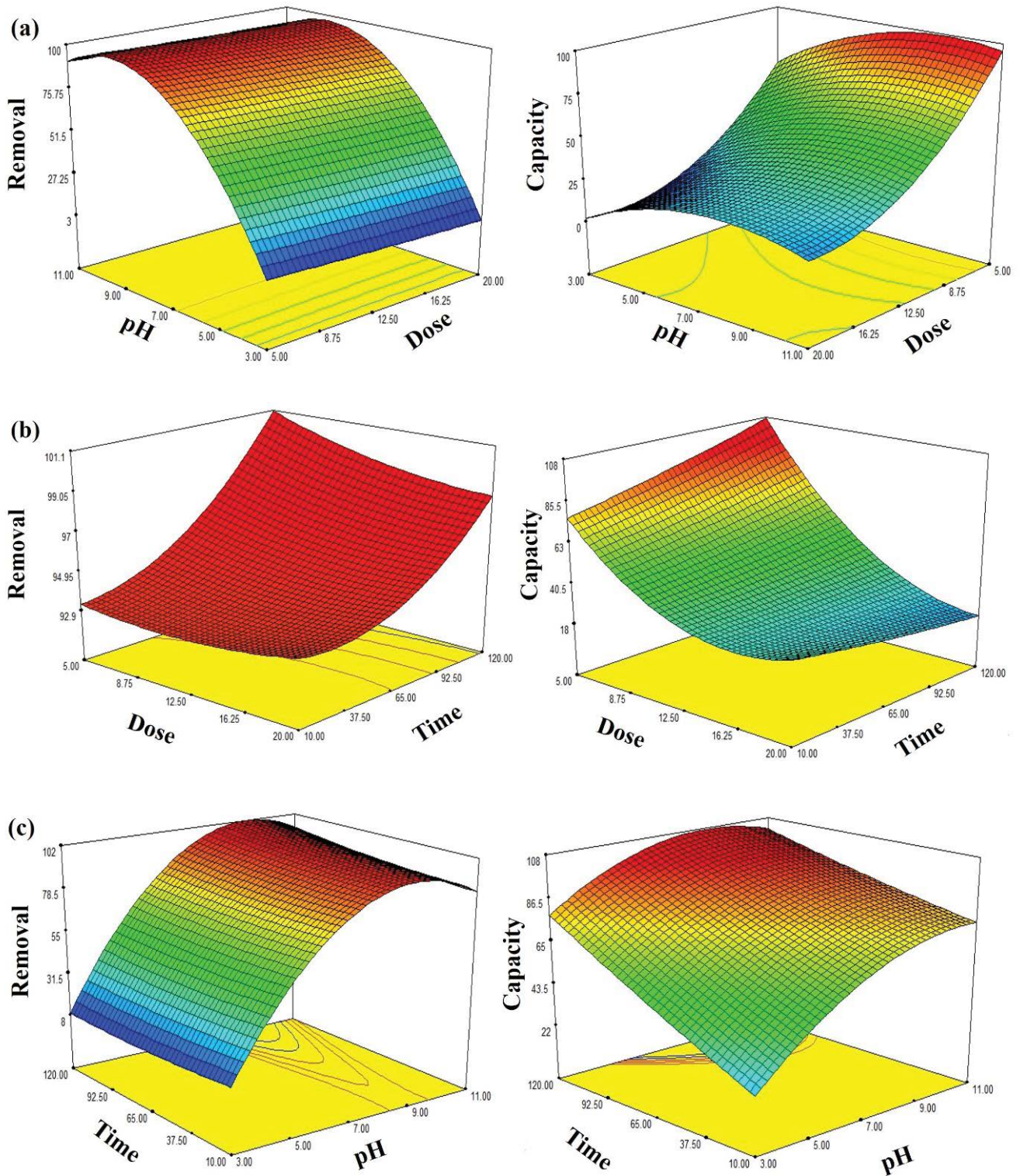


Fig. 5. Surface response plots interaction effects of Al^{3+} adsorption, (a) pH and MWCNTs dose, (b) MWCNTs dose and contact time, and (c) pH and contact time.

with the removal when the pH and contact time are fixed. The capacity decreases when the adsorbent dosage increases. It is possible that this finding is due either to the raised adsorption dosage and conglomeration or to an overlap in the active adsorption sites [37,38].

Fig. 5c presents the results pertaining to the impacts of the interaction between the pH and the contact time of the Al^{3+} adsorption processes on the MWCNTs. Both the removal (%) and the capacity (mg/g) directly correlate with time because the system did not achieve equilibrium. Removal (%) is increased when the pH reaches 10 and decreases in accordance with the decrease in pH. The capacity (mg/g) reaches its maximum at pH 4 and is stabilized [33].

Heavy metals are acknowledged precipitates when pH values are elevated [23,39]. A certain amount of Al in the solution is precipitated in the form of Al^{3+} (NO_3) due to the effect of OH^- anions present in the solution [40]. The initial concentration is measured after adjusting the pH. The effects of precipitation on the capacity and removal of MWCNTs are minimum. Irrespective of the precipitation, the overall number of H^+ cations decreases in accordance with the increase in pH, indicating that they are competing with the Al^{3+} cations to occupy the active sites on the adsorbent. The surface charge of adsorbents is enhanced when the pH is raised [41].

3.3. Adsorption studies

3.3.1. Kinetic study

Kinetic studies are conducted to determine the performance of the MWCNTs adsorbent reaction. For this experimental data, three kinetic models are used including,

pseudo-first-order, pseudo-second-order and the intraparticle diffusion model [42,43]. To conduct the kinetic study, the selected Al^{3+} varies in the concentrations from 3 to 5 mg/L, whereas the absorption dosage value is fixed at a 5 mg and pH of 10 at different time intervals during the time that the equilibrium state is attained. An evaluation of the three models reveals that the pseudo-second-order fits better at various Al^{3+} concentrations, which is expressed by a higher correlation coefficient R^2 . Fig. 6 presents the outcomes of the pseudo-second-order, whilst Table 4 illustrates the results of the applied kinetic models.

3.3.2. Isotherm study

The Langmuir and Freundlich isotherm models are employed in order to examine the adsorption of Al^{3+} in relation to the MWCNTs adsorbent surface. This requires the evaluation of various Al^{3+} concentrations of 3, 5, 10, 20, 30 and 40 ppm using pH 10 and a MWCNTs dosage of 5 mg, which are indicated through an optimization study. These are employed to investigate the adsorption isotherm study [18]. The findings emerging in connection with the isotherm models are displayed in Fig. 7. In accordance with these results, the adsorption of Al^{3+} on MWCNTs surface comprises a better fit in respect of the Langmuir model. Specifically, the Langmuir R^2 model value is 0.993, which is higher than that for the Freundlich model, which is 0.6306. The high adsorption capacity of 393.52 mg/g suggests that the adsorption of Al^{3+} occurs on a homogeneous surface where there is an interaction between the molecules of the adsorbent [44]. The comparison of the maximum capacities of the Al^{3+} removal with the various adsorbents, which were used previously, is shown in Table 5.

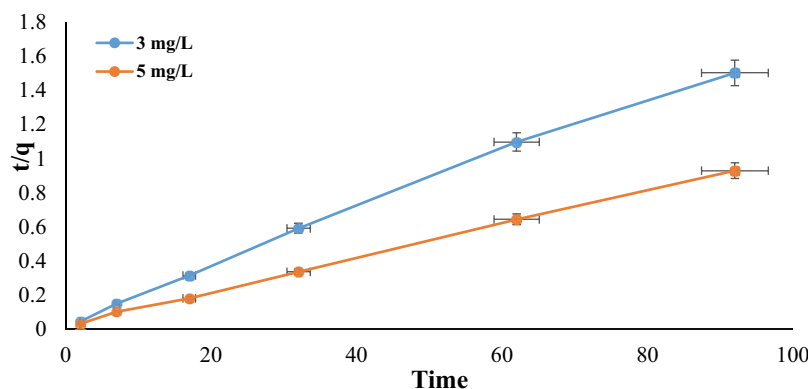


Fig. 6. Plot of pseudo-second-order kinetic for Al^{3+} adsorption on MWCNTs.

Table 4
Adsorption kinetics and correlation coefficient

C_0 (mg/L)	Pseudo-first-order $\ln(q_c - q_t)$ vs time (t)	Pseudo-second-order (t/q_c vs. t)	Intraparticle (q_c vs. $t^{0.5}$)
	R^2	R^2	R^2
3	0.893	0.9968	0.8507
5	0.6932	0.999	0.62

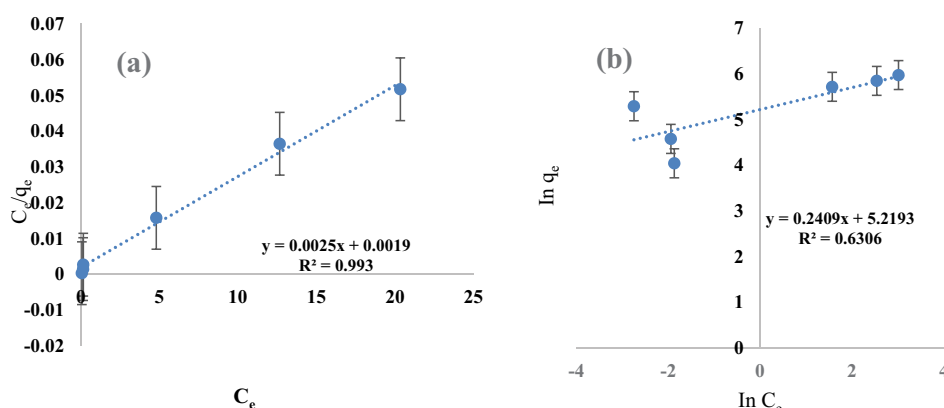


Fig. 7. Plots of isotherm models (a) Langmuir and (b) Freundlich.

Table 5

Comparison of maximum adsorption of Al^{3+} onto different sorbents

Adsorbents	Maximum sorption (mg/g)	References
Multi-walled carbon nanotubes	393.52	This study
MW-Cell-GA	59.8	[45]
Phenol	0.35	[46]
AC/Fe/W	184.12	[47]
Polyacrylonitrile	0.71	[48]
Date pit activated carbon	305	[49]

4. Conclusions

The objective of the current research has been to examine the synthesized MWCNTs grown on PAC impregnated with Fe catalyst (PAC/Fe). This is achieved through the use of acetylene as a carbon source under conditions of 550°C for 47 min. The growth of synthesized MWCNTs was characterized via EDX, FESEM, and TEM. The results of FTIR, XRD, BET, TGA, and zeta potential analysis reveal the graphitic structural formation of MWCNTs, indicating that they comprise a good adsorbent. The optimal parameters for Al^{3+} adsorption are utilized through RSM for MWCNTs under a 5 mg/g dosage, pH 10, and with a 120 min contact time. The adsorption kinetic and isotherm models of adsorption are effectively described using both the pseudo-second-order and the Langmuir models, respectively. The maximum adsorption capacity is 347.88 mg/g. The high-quality structure of MWCNTs can be attributed to the supported catalyst (Fe) on the PAC substrate. The MWCNTs on the PAC/Fe, which are synthesized from agricultural waste, can be used as a low-cost adsorbent and can be expanded in the treatment of other pollutants in wastewater and for several other purposes.

Acknowledgment

The authors gratefully acknowledge Universiti Kebangsaan Malaysia and Universiti of Malaya for technical measurements support.

References

- [1] M. Mishra, M.S. Chauhan, Biosorption as a Novel Approach for Removing Aluminum from Water Treatment Plant Residual—A Review, V.P. Singh, S. Yadav, R.N. Yadava, Eds., Water Quality Management, Springer, Singapore, 2018, pp. 93–99.
- [2] D. Popugaeva, K. Manoli, K. Kreyman, A.K. Ray, Removal of aluminum from aqueous solution by adsorption on montmorillonite K_{10} , TiO_2 , and SiO_2 : kinetics, isotherms, and effect of ions, *Adsorption*, 25 (2019) 1575–1583.
- [3] A.A. Al-Raad, M.M. Hanafiah, A.S. Naje, M.A. Ajeel, A.O. Basheer, T. Ali Aljayashi, M. Ekhwan Toriman, Treatment of saline water using electrocoagulation with combined electrical connection of electrodes, *Processes*, 7 (2019) 242.
- [4] Y. Huang, X.F. Zeng, L.L. Guo, J.H. Lan, L.L. Zhang, D.P. Cao, Heavy metal ion removal of wastewater by zeolite-imidazolate frameworks, *Sep. Purif. Technol.*, 194 (2018) 462–469.
- [5] L. Fang, L. Li, Z. Qu, H.M. Xu, J.F. Xu, N.Q. Yan, A novel method for the sequential removal and separation of multiple heavy metals from wastewater, *J. Hazard. Mater.*, 342 (2018) 617–624.
- [6] W.L. Ang, A.W. Mohammad, D. Johnson, N. Hilal, Forward osmosis research trends in desalination and wastewater treatment: a review of research trends over the past decade, *J. Water Process Eng.*, 31 (2019) 100886, <https://doi.org/10.1016/j.jwpe.2019.100886>.
- [7] S.N.A. Mohd-Salleh, N.S. Mohd-Zin, N. Othman, A review of wastewater treatment using natural material and its potential as aid and composite coagulant, *Sains Malaysiana*, 48 (2019) 155–164.
- [8] P.S. Thue, G.S. dos Reis, E.C. Lima, J.M. Sieliechi, G.L. Dotto, A.G.N. Wamba, S.L.P. Dias, F.A. Pavan, Activated carbon obtained from sapelli wood sawdust by microwave heating for *o*-cresol adsorption, *Res. Chem. Intermed.*, 43 (2017) 1063–1087.
- [9] S. Kizito, S.B. Wu, W.K. Kirui, M. Lei, Q.M. Lu, H. Bah, R.J. Dong, Evaluation of slow pyrolyzed wood and rice husks biochar for adsorption of ammonium nitrogen from piggery manure anaerobic digestate slurry, *Sci. Total Environ.*, 505 (2015) 102–112.
- [10] K. Intani, S. Latif, A.K.M. Rafayatul Kabir, J. Müller, Effect of self-purging pyrolysis on yield of biochar from maize cobs, husks and leaves, *Bioresour. Technol.*, 218 (2016) 541–551.
- [11] H. Zhao, W. Sun, X.M. Wu, B. Gao, The properties of the self-compacting concrete with fly ash and ground granulated blast furnace slag mineral admixtures, *J. Cleaner Prod.*, 95 (2015) 66–74.
- [12] A.O. Basheer, M.M. Hanafiah, M.A. Alsaadi, W.Z. Wan Yaacob, Y. Al-Douri, Synthesis, characterization, and analysis of hybrid carbon nanotubes by chemical vapor deposition: application for aluminum removal, *Polymers*, 12 (2020) 1305, <https://doi.org/10.3390/polym12061305>.

- [13] G.L. Chen, X.M. Liu, P.C. Brookes, J.M. Xu, Opportunities for phytoremediation and bioindication of arsenic contaminated water using a submerged aquatic plant: *Vallisneria spiralis* (Lour.) Hara, *Int. J. Phytorem.*, 17 (2015) 249–255.
- [14] C.C. Murray, H. Vatankhah, C.A. McDonough, A. Nickerson, T.T. Hedtke, T.Y. Cath, C.P. Higgins, C.L. Bellona, Removal of per- and polyfluoroalkyl substances using super-fine powder activated carbon and ceramic membrane filtration, *J. Hazard. Mater.*, 366 (2019) 160–168.
- [15] K.K. Sadasivuni, J.-J. Cabibihan, K. Deshmukh, S. Goutham, M.K. Abubasha, J.P. Gogoi, I. Klemenoks, G. Sakale, B.S. Sekhar, P.S. Rama Sreekanth, K. Venkateswara Rao, M. Knite, A review on porous polymer composite materials for multifunctional electronic applications, *Polym. Plast. Technol. Mater.*, 58 (2019) 1253–1294.
- [16] X. Xiang, L. Zhang, H.I. Hima, F. Li, D.G. Evans, Co-based catalysts from Co/Fe/Al layered double hydroxides for preparation of carbon nanotubes, *Appl. Clay Sci.*, 42 (2009) 405–409.
- [17] M.M. Aljumaily, M.A. Alsaadi, N.A. Hashim, Q.F. Alsahly, F.S. Mjalli, M.A. Atieh, A. Al-Harrasi, PVDF-co-HFP/superhydrophobic acetylene-based nanocarbon hybrid membrane for seawater desalination via DCMD, *Chem. Eng. Res. Des.*, 138 (2018) 248–259.
- [18] H.M. Alayan, M.A. Alsaadi, M.K. AlOmar, M.A. Hashim, Growth and optimization of carbon nanotubes in powder activated carbon for an efficient removal of methylene blue from aqueous solution, *Environ. Technol.*, 40 (2019) 2400–2415.
- [19] A. Yahyazadeh, B. Khoshandam, Carbon nanotube synthesis via the catalytic chemical vapor deposition of methane in the presence of iron, molybdenum, and iron–molybdenum alloy thin layer catalysts, *Results Phys.*, 7 (2017) 3826–3837.
- [20] Y. Zhao, J.H. Choi, P. Kim, W.D. Fei, C.J. Lee, Large-scale synthesis and characterization of super-bundle single-walled carbon nanotubes by water-assisted chemical vapor deposition, *RSC Adv.*, 5 (2015) 30564–30569.
- [21] G.H. Chen, R.C. Davis, H. Kimura, S. Sakurai, M. Yumura, D.N. Futaba, K. Hata, The relationship between the growth rate and the lifetime in carbon nanotube synthesis, *Nanoscale*, 7 (2015) 8873–8878.
- [22] A.A. Mamun, F.R. Ma'an, A.K. Zahirah, M.A. Yehya, A.R.S. Mohammed, M.Z. Alam, S.A. Muyibi, I.A. Faris, I. Azni, Optimisation of arsenic adsorption from water by carbon nanofibers grown on powdered activated carbon impregnated with nickel, *J. Appl. Sci.*, 9 (2009) 3180–3183.
- [23] A.O. Basheer, M.M. Hanafiah, M. Abdulhakim Alsaadi, Y. Al-Douri, M.A. Malek, M. Mohammed Aljumaily, S. Saadi Fiyadh, Synthesis and characterization of natural extracted precursor date palm fibre-based activated carbon for aluminum removal by RSM optimization, *Processes*, 7 (2019) 249, <https://doi.org/10.3390/pr7050249>.
- [24] M.M. Aljumaily, M.A. Alsaadi, N.A. Hashim, Q.F. Alsahly, R. Das, F. Mjalli, Embedded high-hydrophobic CNMs prepared by CVD technique with PVDF-co-HFP membrane for application in water desalination by DCMD, *Desal. Water Treat.*, 142 (2019) 37–48.
- [25] L.S. Krishna, K. Soontarapa, N.K. Asmel, M.A. Kabir, A. Yuzir, W.Z.W. Zuhairi, Y. Sarala, Adsorption of acid blue 25 from aqueous solution using zeolite and surfactant modified zeolite, *Desal. Water Treat.*, 150 (2019) 348–360.
- [26] T. Robshaw, S. Tukra, D.B. Hammond, G.J. Leggett, M.D. Ogden, Highly efficient fluoride extraction from simulant leachate of spent potlining via La-loaded chelating resin. An equilibrium study, *J. Hazard. Mater.*, 361 (2019) 200–209.
- [27] A. Syafiuddin, S. Salmiati, T. Hadibarata, A.B.H. Kueh, M.R. Salim, M.A.A. Zaini, Silver nanoparticles in the water environment in Malaysia: inspection, characterization, removal, modeling, and future perspective, *Sci. Rep.*, 8 (2018) 986, <https://doi.org/10.1038/s41598-018-19375-1>.
- [28] M.M. Aljumaily, M.A. Alsaadi, R. Das, S.B.A. Hamid, N.A. Hashim, M.K. AlOmar, H.M. Alayan, M. Novikov, Q.F. Alsahly, M.A. Hashim, Optimization of the synthesis of superhydrophobic carbon nanomaterials by chemical vapor deposition, *Sci. Rep.*, 8 (2018) 2778, <https://doi.org/10.1038/s41598-018-21051-3>.
- [29] V. Țucureanu, A. Matei, A.M. Avram, FTIR spectroscopy for carbon family study, *Crit. Rev. Anal. Chem.*, 46 (2016) 502–520.
- [30] V.K. Gupta, S. Agarwal, T.A. Saleh, Synthesis and characterization of alumina-coated carbon nanotubes and their application for lead removal, *J. Hazard. Mater.*, 185 (2011) 17–23.
- [31] X. Rodiles, V. Reguero, M. Vila, B. Alemán, L. Arévalo, F. Fresno, V. de la Peña O'Shea, J.J. Vilatela, Carbon nanotube synthesis and spinning as macroscopic fibers assisted by the ceramic reactor tube, *Sci. Rep.*, 9 (2019) 9239.
- [32] H.X. Ou, Q.H. Chen, G.H. Chen, L. Wang, Y.Z. Xu, J.F. Ma, L.P. Wang, Characterization and performance of hollow silica for adsorption of amoxicillin in aqueous solutions, *Water Environ. Res.*, 89 (2017) 348–356.
- [33] N.A. Zarime, W.Z.W. Yaacob, H. Jamil, Decolourization of anionic dye by activated carbon-supported nano-zero valent iron (nZVI), *Chem. Eng. Trans.*, 73 (2019) 85–90.
- [34] P. Liu, Q. Ru, P.M. Zheng, Z.L. Shi, Y. Liu, C.Q. Su, X.H. Hou, S.C. Su, F.C.-C. Ling, One-step synthesis of Zn₂GeO₄/CNT-O hybrid with superior cycle stability for supercapacitor electrodes, *Chem. Eng. J.*, 374 (2019) 29–38.
- [35] M.K. AlOmar, M.A. Alsaadi, M. Hayyan, S. Akib, R.K. Ibrahim, M.A. Hashim, Lead removal from water by choline chloride based deep eutectic solvents functionalized carbon nanotubes, *J. Mol. Liq.*, 222 (2016) 883–894.
- [36] C.L. Ngan, M. Basri, F.F. Lye, H.R.F. Masoumi, M. Tripathy, R.A. Karjiban, E. Abdul-Malek, Comparison of Box–Behnken and central composite designs in optimization of fullerene loaded palm-based nano-emulsions for cosmeceutical application, *Ind. Crops Prod.*, 59 (2014) 309–317.
- [37] G. Halder, K. Sinha, S. Dhawane, Defluoridation of wastewater using powdered activated carbon developed from *Eichhornia crassipes* stem: optimization by response surface methodology, *Desal. Water Treat.*, 56 (2015) 953–966.
- [38] M.K. AlOmar, M.A. Alsaadi, M. Hayyan, S. Akib, M. Ibrahim, M.A. Hashim, Allyl triphenyl phosphonium bromide based DES-functionalized carbon nanotubes for the removal of mercury from water, *Chemosphere*, 167 (2017) 44–52.
- [39] H.B. Bradl, Adsorption of heavy metal ions on soils and soils constituents, *J. Colloid Interface Sci.*, 277 (2004) 1–18.
- [40] A.S.K. Kumar, S.-J. Jiang, Chitosan-functionalized graphene oxide: a novel adsorbent an efficient adsorption of arsenic from aqueous solution, *J. Environ. Chem. Eng.*, 4 (2016) 1698–1713.
- [41] H.M. Alayan, M.A. Alsaadi, A. Abo-Hamad, M.K. AlOmar, M.M. Aljumaily, R. Das, M.A. Hashim, Hybridizing carbon nanomaterial with powder activated carbon for an efficient removal of bisphenol A from water: the optimum growth and adsorption conditions, *Desal. Water Treat.*, 95 (2017) 128–143.
- [42] S.S. Li, H.J. Zhang, S.Y. Hu, J. Liu, Q. Zhu, S.W. Zhang, Synthesis of hierarchical porous carbon in molten salt and its application for dye adsorption, *Nanomaterials*, 9 (2019) 1098, [doi: 10.3390/nano9081098](https://doi.org/10.3390/nano9081098).
- [43] S.K. Lakkaboyana, S. Khantong, N.K. Asmel, A. Yuzir, W.Z.W. Yaacob, Synthesis of copper oxide nanowires-activated carbon (AC@CuO-NWs) and applied for removal methylene blue from aqueous solution: kinetics, isotherms, and thermodynamics, *J. Inorg. Organomet. Polym. Mater.*, 29 (2019) 1658–1668.
- [44] X.Y. Shi, B. Gong, S.J. Liao, J.L. Wang, Y.H. Liu, T.Y. Wang, J.K. Shi, Removal and enrichment of Cr(VI) from aqueous solutions by lotus seed pods, *Water Environ. Res.*, 92 (2020) 84–93.
- [45] W.I. Mortada, I.M.M. Kenawy, Y.G.A. El-Reash, A.A. Mousa, Microwave assisted modification of cellulose by gallic acid and its application for removal of aluminum from real samples, *Int. J. Biol. Macromol.*, 101 (2017) 490–501.
- [46] S.M. Safwat, M. Medhat, H. Abdel-Halim, Adsorption of phenol onto aluminum oxide and zinc oxide: a comparative study with titanium dioxide, *Sep. Sci. Technol.*, 54 (2019) 2840–2852.

- [47] T.A. Saleh, M. Tuzen, A. Sari, Magnetic activated carbon loaded with tungsten oxide nanoparticles for aluminum removal from waters, *J. Environ. Chem. Eng.*, 5 (2017) 2853–2860.
- [48] Z. Aly, A. Graulet, N. Scales, T. Hanley, Removal of aluminum from aqueous solutions using PAN-based adsorbents: characterisation, kinetics, equilibrium and thermodynamic studies, *Environ. Sci. Technol.*, 21 (2014) 3972–3986.
- [49] S.A. Al-Muhtaseb, M.H. El-Naas, S. Abdallah, Removal of aluminum from aqueous solutions by adsorption on date-pit and BDH activated carbons, *J. Hazard. Mater.*, 158 (2008) 300–307.